NAMT
94-003

Algorithms for Computing Motion By Mean Curvature

Noel J. Walkington
Carnegie Mellon University

Research Report No. 94-NA-003

January 1994

Sponsors

U.S. Army Research Office
Research Triangle Park
NC 27709

National Science Foundation
1800 G Street, N.W.
Washington, DC 20550

Algorithms for Computing Motion by Mean Curvature

Noel J. Walkington*

Abstract. We propose a finite element algorithm for computing the motion of a surface moving by mean curvature. The algorithm uses the level set formulation, so that changes in topology of the surface can be accommodated. Stability is deduced by showing that the discrete solutions satisfy both L^∞ and $W^{1,1}$ bounds. Existence of discrete solutions and connections with Brakke flows are established. Some numerical examples and application to related problems, such as the phase field equations, are also presented.

1. Introduction. We consider the numerical solution of problems that involve computing an interface whose motion is governed by its mean curvature. The most elementary example is to determine the motion of a surface whose normal velocity is proportional to it's mean curvature. We will always describe the position of such a surface by the zero set of a function. This idea was introduced in the physics literature [33] and first used as a computational procedure by Osher and Sethian [32]. An elementary calculation shows that the level sets of a function u satisfying the equation

$$\frac{1}{|\nabla u|}\frac{du}{dt} = \nabla\cdot\left(\frac{\nabla u}{|\nabla u|}\right) = \frac{1}{|\nabla u|}\left(I - \frac{\nabla u\otimes\nabla u}{|\nabla u|^2}\right)\cdot D^2 u, \tag{1}$$

will move with velocity equal to mean curvature. This is of great practical value, since the alternative of calculating intrinsic derivatives on a discretized surface is not a tractable problem. A surface moving by mean curvature may develop singularities (causing a change in topology etc.). When such singularities develop, the classical description of the problem involving intrinsic derivatives no longer makes sense; however, by accepting weak solutions of (1), the level set solutions can be continued past singularities to arbitrary times. Indeed, the viscosity solution technique has be used to establish the existence of unique weak solutions of (1) for all times [9, 18, 37]. Moreover, numerical simulations based upon (1) have been used to calculate solutions past the onset of singularities [10, 32, 35],

The viscosity solution technique relies pivotally upon the the presence of a maximum principle for the underlying equation. It was shown by Barles and Souganidis [3] that numerical schemes also satisfying a maximum principle will converge to the unique viscosity solution under very mild additional assumptions. Unfortunately there is no known discretization of (1) that satisfies a discrete maximum principle; indeed, there doesn't appear to be an unambiguously natural discretization for the mean curvature equation. Moreover, there has been almost no analysis of any of the the discrete schemes proposed. Below we present several related numerical scheme for the solution of (1), and show that they are stable in the sense that an $L^\infty(\Omega)$ bound on the initial data be inherited by the solution at all times, and the solutions will also be bounded in $W^{1,1}(Q)$, the Sobolev space of functions with integrable first derivatives defined on

* Department of Mathematics, Carnegie Mellon University, Pittsburgh, PA 15213. The author was supported by National Science Foundation Grant No. DMS-9203406 while this work was undertaken. This work was also supported by the Army Research Office and National Science Foundation through the Center for Nonlinear Analysis.

the space–time cylinder $Q = \Omega \times (0, T)$. This latter bound shows that a sub–sequence of the solutions will converge strongly in $L^1(Q)$, which is often sufficient to establish convergence of distributional solutions of equations; however, currently there are no results in this direction for solutions defined in the viscosity sense. These bounds for the mean curvature equation follow from their divergence structure, that is, the first equality in equation (1); indeed, it is this form of the equation that suggest our numerical scheme. However, the existence theory exploits the second equality in (1), which implies a maximum principle from which stronger $W^{1,\infty}(Q)$ bounds can be deduced.

We briefly review the existence theory for the motion of a surface by it's mean curvature. The most complete theory for (1) is developed using viscosity solutions. Prior to this, classical techniques from parabolic equations had used to obtain smooth solutions (see e.g. Angenent [1]), which may only exist for short times in dimensions greater than two. The viscosity technique was first introduced by Crandall and Lions [12] for first order equations. Jenson [26] established the crucial maximum principle, extending the viscosity technique to second order equations. Subsequently, Chen, Giga and Goto [9] and Evans and Spruck [18] exploited these ideas to obtain unique generalized solutions for (1) that exist for all times to and beyond the onset of singularities. An alternative weak notion for the motion of a surface by it curvature was introduced by Brakke [4]. Brakke associates the surface with a varifold, and essentially integrates by parts to obtain a weak formulation of motion by mean curvature that uses the Radon Nikodym derivative to relax the traditional smoothness assumptions necessary to define curvature. While Brakke obtains the existence of solutions, there is no uniqueness. Examples of non–uniqueness are easily constructed from examples where the viscosity technique gives fat level sets; that is, where the level sets of the solution develop interior. A definition of motion by mean curvature, motivated by formal asymptotic expansions, was proposed in [5] and [14]. The idea is to approximate the surface as the level set of the solution of a parabolic equation containing a small parameter, such as the Allen–Cahn equation. Formally, the zero set will converge to a surface moving by mean curvature as the parameter goes to zero. Subsequent to the development of viscosity and Brakke solutions, it was shown that this process is justified in the sense that it recovers both viscosity and Brakke solutions [17, 25],

A broad spectrum of approaches have been used to numerically approximate the motion of a surface by mean curvature. The most direct approach is to attempt to parameterize the surface. This technique, similar to front tracking in hyperbolic problems, encounters serious problems, since the solutions loose regularity in finite time. Roosen and Taylor [34] developed a method the approximates a curve moving by mean curvature in the plane by line segments (facets) using this approach. When the curve is a graph, Girao and Kohn [22, 21] have shown that such faceted approximations converge. An alternative to discretizing the surface is to assume that it may be represented by a graph. The advantage of this technique is that the classical theory for parabolic equations can be used to obtain smooth solutions prior to the onset of singularities. Recently Decklnick and Dziuk [13] have shown that a discrete space, continuous time, finite element algorithm will exhibit optimal rates of convergence while the solution remains smooth. The method of choice for problems that involve change of topology are level set algorithms based upon direct discretization of (1) [10, 32, 35, 36, 2]. While such algorithms appear to give acceptable solutions, there

are practical problems associated discretizing the problem when certain gradients vanish. Frequently such details are only discussed in a vague fashion, as are existence and stability of the discrete solutions. To date, no convergence theory for approximations of (1) has been established. However, Nochetto, Paolini and Verdi [31] have shown that level sets of numerical approximations of the Allen–Cahn equation do converge to a surface moving by mean curvature, as the parameters tend to zero. In [16], Evans shows that a continuous space, discrete time scheme converges to the viscosity solution of (1). The idea of this scheme is to show that judicious truncations of solutions to the heat equation will generate the correct semi–group.

In Section 2 below, we introduce several related schemes for the approximation of (1). The schemes are designed to inherit a natural energy estimate satisfied by (1), and are similar in spirit to approximations of the minimal surface equation given in [27]. By developing explicit difference formulae for the schemes, we identify modifications and/or restrictions on the mesh that will guarantee the the discrete solutions will also satisfy $L^\infty(\Omega)$ bounds. To keep the ideas clear, all of the estimates in Section 2 are obtained formally, and we postpone until Section 3 the technical details required to justify the formal calculations. Section 4 shows that one of our schemes generates a discrete Brakke flow. Section 5 exhibits some numerical experiments, and in Section 6 we discuss how our ideas can be extended to other problems involving motion by mean curvature.

2. Numerical Schemes for the Mean Curvature Equation. We consider solutions of the mean curvature equation (1) on a bounded domain, Ω, with Dirichlet boundary conditions. Proceeding formally, we multiply (1) by a smooth function, v, vanishing on the boundary and integrate to get

$$\int_\Omega \frac{u_t}{|\nabla u|} v + \frac{\nabla u \cdot \nabla v}{|\nabla u|} = 0. \tag{2}$$

It is this weak form of the equation motivates our spatial discretization. Note that

$$\frac{d}{dt}|\nabla u| = \frac{\nabla u \cdot \nabla u_t}{|\nabla u|},$$

so setting $v = u_t$ gives

$$\int_\Omega \frac{u_t^2}{|\nabla u|} + \frac{d}{dt}\int_\Omega |\nabla u| = 0.$$

Integrating over time gives gives the basic energy estimate

$$\|\nabla u(t)\|_{L^1(\Omega)} + \int_0^T \int_\Omega \frac{u_t^2}{|\nabla u|} = \|\nabla u_0\|_{L^1(\Omega)},$$

showing that the $W^{1,1}(\Omega)$ semi–norm decays. The desire to retain this estimate motivates our temporal discretization[1].

In order to discretize (2), we introduce a triangulation, $\mathcal{T}_h$, of the domain Ω, where $h > 0$ denotes the diameter of the largest simplex in $\mathcal{T}_h$. Denote by V_h the space of

[1] The author is indebted to Y. Giga for suggesting that a scheme should satisfy this estimate in addition to the $L^\infty(\Omega)$ estimates established below.

piecewise linear function defined on $\mathcal{T}_h$ vanishing on the boundary $\partial\Omega$, and let $\tau > 0$ be a time step size. Letting $u^n \in V_h$ denote an approximation of $u(n\tau)$, we can introduce a (formally) second order approximation of (2) by requiring $u^{n+1} \in V_h$,

$$\int_\Omega \frac{2}{\tau}\frac{u^{n+1}-u^n}{|\nabla u^{n+1}|+|\nabla u^n|}v + \frac{(\nabla u^{n+1}+\nabla u^n)\cdot\nabla v}{|\nabla u^{n+1}|+|\nabla u^n|} = 0, \qquad \forall\, v \in V_h. \tag{3}$$

Given that (generalized) solutions of this problem do exist, substituting $v = u^{n+1} - u^n$ shows that this scheme satisfies the following discrete version of the $W^{1,1}$ estimate:

$$\|\nabla u^n\|_{L^1(\Omega)} + \sum_{m=0}^{n-1} \tau \int_\Omega \frac{2}{\tau^2}\frac{(u^{m+1}-u^m)^2}{|\nabla u^{m+1}|+|\nabla u^m|} = \|\nabla u^0\|_{L^1(\Omega)}. \tag{4}$$

An estimate on the time derivative follows from

$$\begin{aligned}
\int_0^T \|u_t(t)\|_{L^1(\Omega)} &= \sum_{m=0}^{n-1} \tau \|(u^{m+1}-u^m)/\tau\|_{L^1(\Omega)} \\
&= \sum_{m=0}^{n-1} \tau \int_\Omega \frac{|u^{m+1}-u^m|}{\tau(|\nabla u^{m+1}|+|\nabla u^m|)^{1/2}}(|\nabla u^{m+1}|+|\nabla u^m|)^{1/2} \\
&\le \sum_{m=0}^{n-1} \tau \left(\int_\Omega \frac{2(u^{m+1}-u^m)^2}{\tau^2(|\nabla u^{m+1}|+|\nabla u^m|)}\right)^{1/2} \left(\frac{1}{2}\int_\Omega |\nabla u^{m+1}|+|\nabla u^m|\right)^{1/2} \\
&\le \sqrt{T}\|\nabla u^0\|_{L^1(\Omega)}.
\end{aligned}$$

It is well known that discretizations like (3) will not generate solutions with $L^\infty(\Omega)$ norms bounded by that of the initial data. In order to obtain such bounds it is usually necessary to modify the spatial and/or temporal terms. Below we show that the first order scheme

$$\int_\Omega \frac{1}{\tau}\frac{u^{n+1}-u^n}{|\nabla u^{n+1}|+|\nabla u^n|}v + \frac{\nabla u^{n+1}\cdot\nabla v}{|\nabla u^{n+1}|+|\nabla u^n|} = 0, \qquad \forall\, v \in V_h, \tag{5}$$

obtained by making the numerator of the spatial term in (3) implicit, will satisfy $L^\infty(\Omega)$ bounds on suitably chosen meshes (cf. [11]). Diagonal approximations of the temporal term, discussed below, will establish $L^\infty(\Omega)$ bounds on a broader class of meshes. These two modifications will not alter the apriori bounds established above, except that the equality in (4) becomes an inequality. We chose to motivate these modifications using the complementary volume (co–volume) algorithm. This algorithm has the advantage that it will enable us to concisely write down explicit finite difference equations corresponding to (3).

2.1. Dual Meshes. Given a triangulation of a bounded domain $\Omega \subset \Re^n$ ($n = 2$ or 3), we can construct a dual (non–simplicial) mesh. Each cell, V_i, of the dual mesh is associated with a node $\mathbf{x}_i$ of $\mathcal{T}_h$, and is bounded by the lines (planes) that bisect and are perpendicular to the edges emanating from the node (see Figure 1). The dual cell associated with a particular node can also be characterized as the set of points in Ω that are closer to that node than any other. The perpendicular bisectors will meet at the circumcenters of the simplicies of $\mathcal{T}_h$ which form the nodes of the complementary mesh. We will refer to the edges, nodes etc. of the dual mesh as co–edges, co–nodes

etc. While it is possible to modify an arbitrary triangulation so that the co–edges do not self intersect, we will restrict ourselves to triangulations whose interior angles are no greater than $\pi/2$. This guarantees that the circumcenter of a simplex will be contained within the simplex, and co–edges intersect only at the co–nodes.

We will denote the edge of $\mathcal{T}_h$ connecting the i^{th} node to the j^{th} by σ_{ij}, and its length by h_{ij}. Similarly, σ'_{ij} will denote the co–edge (co–plane) that is the perpendicular bisector of σ_{ij}, and h'_{ij} will denote its length (area). We denote by $\mathcal{E}_{ij}$ the set of simplicies having σ_{ij} as an edge: $\mathcal{E}_{ij} = \{T \in \mathcal{T}_h \mid \sigma_{ij} \subset T\}$. Note that in two dimensions, $\mathcal{E}_{ij}$ will generically contain only two simplicies (see Figure 1); the exceptions being the boundary edges that only meet one simplex. For each $T \in \mathcal{E}_{ij}$ we let c_{ij}^T be the length (area) of that portion of σ'_{ij} that in T, i.e. $c_{ij}^T = |\sigma'_{ij} \cap T|$. Let $\mathcal{N}_i$ be the set of simplicies that have the i^{th} node as a vertex, and for each node of $\mathcal{T}_h$ let C_i denote the set of nodes connected to the i^{th} node by an edge. We will let $\sum_i(.)$ and $\sum_{(i,j)}(.)$ denote sums over the nodes of $\mathcal{T}_h$ and the edges of $\mathcal{T}_h$ respectively.

2.2. Co–Volume Discretizations. Co–volume approximations of (1) are motivated by integrating the equation over a co–volume V_i, and integrating by parts.

$$\int_{V_i} \frac{u_t}{|\nabla u|} = \int_{\partial V_i} \frac{1}{|\nabla u|} \frac{\partial u}{\partial n} = \sum_{j \in C_i} \int_{\sigma'_{ij}} \frac{1}{|\nabla u|} \frac{\partial u}{\partial n}.$$

If $u \in V_h$ is piecewise linear, $\partial u/\partial n = (u_j - u_i)/h_{ij}$ on σ'_{ij}, so that

$$\int_{V_i} \frac{u_t}{|\nabla u|} = \sum_{j \in C_i} \left(\int_{\sigma'_{ij}} \frac{1}{|\nabla u|} \right) \frac{u_j - u_i}{h_{ij}}.$$

Noting that the gradient of u is piecewise constant we can write

$$\int_{\sigma'_{ij}} \frac{1}{|\nabla u|} = \sum_{T \in \mathcal{E}_{ij}} \frac{c_{ij}^T}{|\nabla u_T|},$$

where, $|\nabla u_T|$ denotes the gradient of u in the simplex T. The co–volume scheme approximates the first term of the equation by

$$\int_{V_i} \frac{u_t}{|\nabla u|} \simeq |V_i| \frac{(u_i)_t}{|\nabla u_i|},$$

where $u_i = u(x_i)$ is the value at the node, and $|\nabla u_i|$ is an approximation of the gradient at this node. Fully discrete schemes are made by taking a temporal average of these spatial discretizations. In order to obtain a scheme that satisfies the energy estimate we consider

$$|V_i| \frac{u_i^{n+1} - u_i^n}{|\nabla u_i|} + \tau \sum_{j \in C_i} a_{ij}(u^{n+1}, u^n)(u_i^{n+1} - u_j^{n+1}) = 0, \tag{6}$$

where

$$a_{ij}(u, v) = \frac{2}{h_{ij}} \sum_{T \in \mathcal{E}_{ij}} \frac{c_{ij}^T}{|\nabla u_T| + |\nabla v_T|}. \tag{7}$$

Note that the coefficients a_{ij} are symmetric, $a_{ij}(u,v) = a_{ji}(u,v) = a_{ij}(v,u)$, and non-negative. In (6), $|\nabla u_i|$ can be selected as any reasonable approximation of the gradient of u at the i^{th} node. Since the scheme is formally first order, the natural choice is to make this term explicit, eg.

$$|\nabla u_i| = \sum_{T \in \mathcal{N}_i} \frac{|T \cap V_i|}{|V_i|} |\nabla u_T^n|.$$

We show that this scheme has a (generalized) solutions in Section 3.

Since the a_{ij} and $|\nabla u_i|$ are non-negative, it follows that $\|u^n\|_{L^\infty(\Omega)} \leq \|u^0\|_{L^\infty(\Omega)}$. To see this, let u^{n+1} achieve its maximum at node i, then

$$u_i^{n+1} + \frac{\tau}{|V_i|} |\nabla u_i| \sum_{j \in C_i} a_{ij}(u^{n+1}, u^n)(u_i^{n+1} - u_j^{n+1}) = u_i^n.$$

Since the second term on the left is non-negative, it follows that $u_i^{n+1} \leq u_i^n$, so that $\|u^{n+1}\|_{L^\infty(\Omega)} \leq \|u^n\|_{L^\infty(\Omega)}$.

In order to show that solutions of this discrete scheme satisfy discrete $W^{1,1}$ bounds, we will use the following lemma.

LEMMA 2.1. *Let $\mathcal{T}_h$ be a mesh having simplicies with interior angles not exceeding $\pi/2$, and let u, $v \in V_h$, and $\bar{w}$ be piecewise constant on $\mathcal{T}_h$, then*

$$\int_\Omega \bar{w} \nabla u \cdot \nabla v = \sum_i \left(\sum_{j \in C_i} a_{ij}(\bar{w})(u_i - v_j) \right) v_i,$$

where $a_{ij}(\bar{w}) = (1/h_{ij}) \sum_{T \in \mathcal{E}_{ij}} w_T c_{ij}^T$.

The proof is similar to that given in [30], and reduces to considering the identity on one simplex.

Multiplying (6) by $u_i^{n+1} - u_i^n$ and summing over all of the nodes in the mesh gives the energy estimate

$$\|\nabla u^n\|_{L^1(\Omega)} + \sum_{m=0}^{n-1} \left(\tau \sum_i |V_i| \frac{(u_i^{m+1} - u_i^m)^2}{\tau^2 |\nabla u_i^m|} + \int_\Omega \frac{|\nabla(u^{m+1} - u^m)|^2}{|\nabla u^{m+1}| + |\nabla u^m|} \right) = \|\nabla u^0\|_{L^1(\Omega)}. \tag{8}$$

The identity

$$2\nabla u^{n+1} \cdot \nabla(u^{n+1} - u^n) = |\nabla u^{n+1}|^2 - |\nabla u^n|^2 + |\nabla(u^{n+1} - u^n)|^2,$$

used in the derivation of (8), shows the presence of extra dissipation in the first order scheme (c.f. 4). Again this implies a bound on u_t

$$\int_0^T \|\bar{u}_t\|_{L^1(\Omega)} = \sum_{m=0}^{n-1} \tau \sum_i |V_i| \left| \frac{u_i^{m+1} - u_i^m}{\tau} \right| \leq \sqrt{T} \|\nabla u^0\|_{L^1(\Omega)},$$

where $\bar{u}$ denotes the function that is piecewise constant on the co-volumes and taking on the nodal values of u.

While (6) only a first order scheme, this is not inherent in the co–volume algorithm, it is the need to treat the spatial term implicitly that caused a reduction in accuracy. A second order co–volume scheme is

$$(9) \qquad |V_i|\frac{u_i^{n+1}-u_i^n}{|\nabla u_i|}+\frac{\tau}{2}\sum_{j\in C_i}a_{ij}(u^{n+1},u^n)\left((u_i^{n+1}+u_i^n)-(u_j^{n+1}+u_j^n)\right)=0,$$

where we now choose

$$|\nabla u_i|=\frac{1}{2}\sum_{T\in\mathcal{N}_i}\frac{|T\cap V_i|}{|V_i|}\left(|\nabla u_T^{n+1}|+|\nabla u_T^n|\right).$$

Note that it would be very difficult to verify that this scheme was consistent with (1) if Lemma 2.1 were not available to show that the spatial terms in this discretization are exactly the difference equations that result from the spatial terms in (3). This scheme is then a "lumped mass" approximation of (3).

2.3. Difference Equations for the Temporal Terms. Using the following lemma we may write down the discrete equations that arise from (3) and (5).

LEMMA 2.2. *Let $\mathcal{T}_h$ be a triangulation of Ω, and let u and v be piecewise linear functions defined on $\mathcal{T}_h$, and $\bar{w}$ be a piecewise constant function on $\mathcal{T}_h$.*

- *If $\Omega\subset\Re^2$ then*

$$\int_\Omega \bar{w}uv=\sum_i\sum_{j\in C_i}b_{ij}(\bar{w})(u_i+u_j)v_i=\sum_{(i,j)}b_{ij}(\bar{w})(u_i+u_j)(v_i+v_j),$$

  where $b_{ij}(\bar{w})=(1/12)\sum_{T\in\mathcal{E}_{ij}}w_T|T|$.
- *If $\Omega\subset\Re^3$ then*

$$\begin{aligned}\int_\Omega \bar{w}uv &= \sum_i\sum_{j\in C_i}b_{ij}(\bar{w})\left((2/3)u_i+u_j\right)v_i\\ &= \sum_{(i,j)}b_{ij}(\bar{w})\left[((2/3)u_i+u_j)v_i+(u_i+(2/3)u_j)v_j\right],\end{aligned}$$

  where $b_{ij}(\bar{w})=(1/20)\sum_{T\in\mathcal{E}_{ij}}w_T|T|$.

This lemma is proved by simple quadrature. The discrete equations for (3) then become

$$\sum_{j\in C_i}b_{ij}(u^{n+1},u^n)\left(\alpha(u_i^{n+1}-u_i^n)+(u_j^{n+1}-u_j^n)\right)+\frac{\tau}{2}\sum_{j\in C_i}a_{ij}(u^{n+1},u^n)\left((u_i^{n+1}+u_i^n)-(u_j^{n+1}+u_j^n)\right)=0,$$

where $a_{ij}(.,.)$ is given in (7), and

$$b_{ij}(u,v)=\frac{1}{\beta}\sum_{T\in\mathcal{E}_{ij}}\frac{2\,|T|}{|\nabla u_T|+|\nabla v_T|},$$

with $(\alpha,\beta)=(1,12)$ in two dimensions, and $(2/3,20)$ in three dimensions.

The traditional lumped mass approximation to diagonalize the temporal terms may be thought of as approximating $u_j^{n+1} - u_j^n$ by $u_i^{n+1} - u_i^n$ in the above to give

$$\tilde{b}_i(u_i^{n+1} - u_i^n) + \frac{\tau}{2} \sum_{j \in C_i} a_{ij}(u^{n+1}, u^n) \left((u_i^{n+1} + u_i^n) - (u_j^{n+1} + u_j^n) \right) = 0,$$

where

$$\tilde{b}_i = \frac{\alpha + 1}{\beta} \sum_{j \in C_i} \sum_{T \in \mathcal{E}_{ij}} \frac{2\,|T|}{|\nabla u_T^{n+1}| + |\nabla u_T^n|} = \frac{1}{\gamma} \sum_{T \in \mathcal{N}_i} \frac{2\,|T|}{|\nabla u_T^{n+1}| + |\nabla u_T^n|},$$

and $\gamma = 3$ in two dimensions and 4 in three dimensions. Of course this can also be viewed as a vertex quadrature rule assigning a weight of $1/3$ to each of the three nodes of a triangle or $1/4$ to each of the four vertices of a tetrahedron. Note that this diagonalization gives different weights than the co-volume algorithm (6) for non-uniform meshes.

We finish this section by showing that solutions given by (5) will also satisfy $L^\infty(\Omega)$ bounds for suitably chosen meshes. The difference equation for (5) are

$$\sum_{j \in C_i} b_{ij}(u^{n+1}, u^n) \left(\alpha(u_i^{n+1} - u_i^n) + (u_j^{n+1} - u_j^n) \right) + \tau \sum_{j \in C_i} a_{ij}(u^{n+1}, u^n)(u_i^{n+1} - u_j^{n+1}) = 0.$$

Rearranging we obtain

$$(1 + \alpha) \left(\sum_{j \in C_i} b_{ij} \right) u_i^{n+1} + \sum_{j \in C_i} (\tau a_{ij} - b_{ij})(u_i^{n+1} - u_j^{n+1}) = \sum_{j \in C_i} b_{ij} \left(\alpha u_i^n + u_j^n \right),$$

where $b_{ij} = b_{ij}(u^{n+1}, u^n)$, and

$$\begin{aligned} \tau a_{ij} - b_{ij} &= \tau a_{ij}(u^{n+1}, u^n) - b_{ij}(u^{n+1}, u^n) \\ &= \sum_{T \in \mathcal{E}_{ij}} \left(\tau \frac{c_{ij}^T}{h_{ij}} - \frac{|T|}{\beta} \right) \frac{2}{|\nabla u_T^{n+1}| + |\nabla u_T^n|}. \end{aligned}$$

For meshes with all interior angles strictly acute, $c_{ij}^T > 0$, so if the time step τ satisfies

$$\tau \geq \frac{|T| h_{ij}}{\beta c_{ij}^T},$$

for each edge σ_{ij} and $T \in \mathcal{E}_{ij}$, then the coefficients $\tau a_{ij} - b_{ij}$ are all non-negative, implying $\|u^n\|_{L^\infty(\Omega)} \leq \|u^0\|_{L^\infty(\Omega)}$. If all interior angles of the meshes are bounded away from $\pi/2$, then $|T| \sim h^2$ (h^3 in three dimensions), $c_{ij}^T \sim h$ (h^2) and $h_{ij} \sim h$ so that this above condition becomes $\tau > Ch^2$.

2.4. Summary. We summarize the various properties for each of the approximations introduced above.

- Solutions of each of the schemes (3), (5), (6), (9) are bounded in $L^\infty[0, T; W^{1,1}(\Omega)]$ and $W^{1,1}(Q)$ by $\|\nabla u^0\|_{L^1(\Omega)}$ and $\sqrt{T}\|\nabla u^0\|_{L^1(\Omega)}$ respectively.

- Schemes (3) and (9) are formally of second order (in space and time) and schemes (6) and (5) are of first order.
- Solutions of (6) are bounded in $L^\infty(Q)$ with bound depending only upon $\|u^0\|_{L^\infty(\Omega)}$, and for strictly acute meshes with sufficiently large time steps, (5) is similarly bounded.
- Schemes (6) and (5) satisfy the additional bound

$$\sum_{m=1}^{\infty} \int_\Omega \frac{|\nabla(u^{m+1} - u^m)|^2}{|\nabla u^{m+1}| + |\nabla u^m|} \leq \|\nabla u^0\|_{L^1(\Omega)}.$$

In the above, $Q = \Omega \times [0, T]$ is the natural space time cylinder.

3. Existence of Solutions. Clearly the discrete schemes presented above are not well defined when certain gradients vanish. Following [18], we construct generalized solutions of our discrete schemes that are limits of solutions to approximate problems. Existence for the approximate problems is deduced from the following form of Brower's fixed point theorem.

THEOREM 3.1. *Let $F : \Re^n \to \Re^n$ be continuous and suppose that for some $R > 0$ and $y \in B_R(0)$, the ball of radius R centered at zero, $F(x) \cdot (x - y) \geq 0$ on $S_R(0)$, the sphere of radius R centered at the origin. Then F has a zero in $B_R(0)$.*

Notation: 1) For $\epsilon \geq 0$ we let $|\nabla u|_\epsilon$ denote $\sqrt{|\nabla u| + \epsilon^2}$.
2) Given a scheme such as (3), we will denote by $(3)_\epsilon$ the scheme obtained by replacing the gradient terms in the denominators with their ϵ approximates.

LEMMA 3.2. *Let $\mathcal{T}_h$ be a triangulation of the bounded domain $\Omega \subset \Re^n$, and let V_h be the space of piecewise linear functions defined over $\mathcal{T}_h$ vanishing on the boundary of Ω. Given $u^n \in V_h$, each of the schemes $(3)_\epsilon$, $(5)_\epsilon$, $(6)_\epsilon$, and $(9)_\epsilon$ have a solution. Moreover, the solutions of $(3)_\epsilon$ and $(5)_\epsilon$ satisfy*

$$\|u^\epsilon\|_{L^1(\Omega)} + \int_\Omega \frac{2}{\tau} \frac{(u^\epsilon - u^n)^2}{|\nabla u^\epsilon|_\epsilon + |\nabla u^n|_\epsilon} \leq \|u^n\|_{L^1(\Omega)} + \epsilon|\Omega|,$$

and the solutions of $(6)_\epsilon$ and $(9)_\epsilon$ satisfy

$$\|u^\epsilon\|_{L^1(\Omega)} + \sum_i |V_i| \frac{(u_i^\epsilon - u_i^n)^2}{\tau |\nabla u_i|_\epsilon} \leq \|u^n\|_{L^1(\Omega)} + \epsilon|\Omega|.$$

Proof. We only consider the proof for (3), since the others follow similarly. Let N be the number of interior nodes and for each $\epsilon > 0$ define $F : \Re^N \to \Re^N$ by

$$F(\mathbf{u}) \cdot \mathbf{v} = \int_\Omega \frac{2}{\tau} \frac{u - u^n}{|\nabla u|_\epsilon + |\nabla u^n|_\epsilon} v + \frac{(\nabla u + \nabla u^n) \cdot \nabla v}{|\nabla u|_\epsilon + |\nabla u^n|_\epsilon}.$$

In the above we assume an ordering of the nodes of $\mathcal{T}_h$ so that $\mathbf{u} \in \Re^N$ may be identified with $u \in V_h$ in the natural way.

$$\begin{aligned} F(\mathbf{u}) \cdot (\mathbf{u} - \mathbf{u}^n) &= \int_\Omega \frac{2}{\tau} \frac{(u - u^n)^2}{|\nabla u|_\epsilon + |\nabla u^n|_\epsilon} + \frac{|\nabla u|^2 - |\nabla u^n|^2}{|\nabla u|_\epsilon + |\nabla u^n|_\epsilon} \\ &= \int_\Omega \frac{2}{\tau} \frac{(u - u^n)^2}{|\nabla u|_\epsilon + |\nabla u^n|_\epsilon} + |\nabla u|_\epsilon - |\nabla u^n|_\epsilon \\ &\geq \int_\Omega \frac{2}{\tau} \frac{(u - u^n)^2}{|\nabla u|_\epsilon + |\nabla u^n|_\epsilon} + \|u\|_{L^1(\Omega)} - \|u^n\|_{L^1(\Omega)} - \epsilon|\Omega|. \end{aligned}$$

If $\mathbf{u} \in S_R(0)$ where $R > 0$ is chosen sufficiently large to guarantee that $|\mathbf{u}^n| \leq R$ and $\|\nabla u\|_{L^1(\Omega)} \geq \|\nabla u^n\|_{L^1(\Omega)} + \epsilon|\Omega|$, then $F(\mathbf{u}) \cdot (\mathbf{u} - \mathbf{u}^n) \geq 0$. An application of Theorem 3.2 shows that F has a zero $u^\epsilon \in B_R(0)$. Substituting $u = u^\epsilon$ and $F(\mathbf{u}^\epsilon) = 0$ into the above establishes the bound. □

Since the bounds on u^ϵ are independent of ϵ, compactness of balls in $\Re^N$ guarantees that we may pass to a subsequence $u^\epsilon \to u^{n+1}$. It is intuitively clear that these are good candidates for "generalized" solutions; however, it is not clear in what sense they satisfy the discrete mean curvature equation. We address this question in the following theorem.

THEOREM 3.3. *Let $\mathcal{T}_h$ be a triangulation of the bounded domain, Ω, and V_h be the space of piecewise linear functions defined over $\mathcal{T}_h$ that vanish on the boundary. For each of the schemes (3), (5), (6), (9), there is exists $u^{n+1} \in V_h$ and functions $\boldsymbol{\nu}$ and H satisfying*

$$\int_\Omega Hv + \boldsymbol{\nu} \cdot \nabla v = 0 \qquad \forall\, v \in V_h$$

for schemes (3) and (5), and

$$\sum_i |V_i| H_i v_i + \int_\Omega \boldsymbol{\nu} \cdot \nabla v = 0 \qquad \forall\, v \in V_h$$

for schemes (6) and (9), where $\boldsymbol{\nu}$ and H are related to u^{n+1} as follows:

$\boldsymbol{\nu}$ is a piecewise constant vector field defined on $\mathcal{T}_h$. For schemes (3) and (9) and

$$\begin{array}{rcll} \boldsymbol{\nu} & = & \frac{\nabla u^{n+1} + \nabla u^n}{|\nabla u^{n+1}| + |\nabla u^n|} & \text{if the denominator is non-zero} \\ |\boldsymbol{\nu}| & \leq & 1 & \text{otherwise,} \end{array}$$

and for schemes (5) and (6)

$$\begin{array}{rcll} \boldsymbol{\nu} & = & 2\frac{\nabla u^{n+1}}{|\nabla u^{n+1}| + |\nabla u^n|} & \text{if the denominator is non-zero} \\ |\boldsymbol{\nu}| & \leq & 2 & \text{otherwise.} \end{array}$$

For schemes (3) and (5), H is a discontinuous piecewise linear function satisfying

$$H = \frac{2}{\tau} \frac{u^{n+1} - u^n}{|\nabla u^{n+1}| + |\nabla u|} \qquad \text{if the denominator is non-zero,}$$

and for schemes (6) and (9) H is piecewise constant on the co-volumes and satisfies

$$H_i = \frac{u_i^{n+1} - u_i^n}{\tau |\nabla u_i|} \qquad \text{if the denominator is non-zero.}$$

(Recall that $|\nabla u_i|$ is an approximation of $|\nabla u|$ at the i^{th} node.)

Proof. We establish this result by passing to the limit as $\epsilon \to 0$ in the equation for the approximate solutions. Since $\{\|\nabla u^\epsilon\|_{L^1(\Omega)}\}_{\epsilon > 0}$ is bounded independently of ϵ, we may pass to a sub-sequence such that $u^\epsilon \to u^{n+1}$.

Let $\boldsymbol{\nu}^\epsilon$ be defined by

$$\boldsymbol{\nu}^\epsilon = \frac{\nabla u^\epsilon + \nabla u^n}{|\nabla u^\epsilon|_\epsilon + |\nabla u^n|_\epsilon}, \qquad \text{for schemes (3) and (9),}$$

and

$$\boldsymbol{\nu}^\epsilon = 2\frac{\nabla u^\epsilon}{|\nabla u^\epsilon|_\epsilon + |\nabla u^n|_\epsilon}, \qquad \text{for schemes (5) and (6).}$$

On simplicies where the denominator doesn't vanish in the limit, it clear that $\boldsymbol{\nu}^\epsilon$ converges to a function $\boldsymbol{\nu}$ with the same form as $\boldsymbol{\nu}^\epsilon$, except u^{n+1} replaces u^ϵ. On simplicies where the denominator vanishes, ∇u^n must be zero, so that $\boldsymbol{\nu}_T^\epsilon = \nabla u^\epsilon/(|\nabla u^\epsilon|_\epsilon + \epsilon)$ (or $\boldsymbol{\nu}_T^\epsilon = 2\nabla u^\epsilon/(|\nabla u^\epsilon|_\epsilon + \epsilon)$ or the first order schemes) which has modulus less than one (or two for the first order schemes). By passing to a subsequence, we may assume that $\boldsymbol{\nu}^\epsilon$ also converges on these simplicies too, and hence the whole of Ω.

We next consider the temporal term for the lumped mass approximations (6) and (9). Define H^ϵ to be the function that is piecewise constant on the co–volumes and assumes nodal values $H_i^\epsilon = (u_i^\epsilon - u_i^n)/(\tau|\nabla u_i|_\epsilon)$. Selecting $v \in V_h$ with nodal values $v_i = sgn(H_i^\epsilon)$ in the equation satisfied by u^ϵ, where $sgn(.)$ is the signum function ($sgn(s) = 1$ if $s > 0$, -1 if $s < 0$ and 0 if $s = 0$), gives

$$\|H^\epsilon\|_{L^1(\Omega)} = \sum_i |V_i||H_i^\epsilon| = -\int_\Omega \boldsymbol{\nu}^\epsilon \cdot \nabla v \le 2\|\nabla v\|_{L^1(\Omega)} \le 2|\Omega|/h,$$

showing H^ϵ is bounded independently of ϵ. By passing to a subsequence we may assume that the H^ϵ converge, and when the denominator doesn't vanish in the limit it is clear that the limit H has the same form as H^ϵ with u^ϵ replaced by u^{n+1}.

We finally consider the temporal term for (3) and (5). Again it suffices to show that

$$H^\epsilon = \frac{2}{\tau}\frac{u^\epsilon - u^n}{|\nabla u^\epsilon|_\epsilon + |\nabla u^n|_\epsilon}$$

is bounded independently of ϵ; however, the proof is a little more tedious. We begin by observing that H^ϵ is bounded for any simplicies that meet the boundary. Indeed, if $x_0 \in T \cap \partial\Omega$, $u^\epsilon(x) = \nabla u_T^\epsilon \cdot (x - x_0)$ for $x \in T$, implying $|H^\epsilon(x)| \le 2|x - x_0|/\tau \le 2h/\tau$ for $x \in T$. Define the set D by

$$D = \{T \in \mathcal{T}_h \mid \text{there is no subsequence } H_T^\epsilon \to 0,\ |\nabla u^\epsilon|_\epsilon + |\nabla u^n|_\epsilon \to 0, \text{ and } T \cap \partial\Omega = \emptyset\}.$$

It is clear that we may pass to a sub–sequence such that H^ϵ converges on $\Omega \setminus D$; moreover, by passing to a further subsequence, we can assume that H_T^ϵ is bounded away from zero and has one sign for each simplex $T \in D$.

We next claim that we can chose $v \in V_h$ such that $v|_T = sgn(H_T^\epsilon)$ for $T \in D$ and zero at the nodes disjoint from D. To see this, recall that

$$\int_\Omega \frac{2}{\tau}\frac{(u^\epsilon - u^n)^2}{|\nabla u^\epsilon|_\epsilon + |\nabla u^n|_\epsilon} \le \|u^n\|_{L^1(\Omega)} + \epsilon|\Omega|,$$

implying $u_T^\epsilon \to u_T^n$ for each $T \in D$. Also, since $\nabla u_T^n = 0$ for $T \in D$, it follows that u_T^ϵ converges to the constant u_T^n. It now follows that if ϵ sufficiently small, no node can belong to two simplicies T_1 and $T_2 \in D$ having $H_{T_1}^\epsilon$ and $H_{T_2}^\epsilon$ of opposite sign, since this implies u^n changes sign in one of the simplicies, contradicting $\nabla u^n = 0$. Since $\int_\Omega H^\epsilon v + \boldsymbol{\nu}^\epsilon \cdot v = 0$, it follows that

$$\begin{aligned}
\int_D |H^\epsilon| &= \int_D Hv = -\int_{\Omega\setminus D} H^\epsilon v - \int_\Omega \boldsymbol{\nu}^\epsilon \cdot \nabla v \\
&\le \|H^\epsilon\|_{L^1(\Omega\setminus D)} + 2\|\nabla v\|_{L^1(\Omega)} \\
&\le \|H^\epsilon\|_{L^1(\Omega\setminus D)} + 2|\Omega|/h,
\end{aligned}$$

implying H^ϵ is bounded on D and hence all Ω. □

We finish this section by observing that this limiting procedure is similar to that used to obtain viscosity solutions of (1). The definition of a viscosity solution for (1) requires

$$\frac{\partial u}{\partial t} = (I - \boldsymbol{\nu} \otimes \boldsymbol{\nu}) \cdot D^2 u$$

to hold (in the viscosity sense) at points where $|\nabla u| = 0$ for some vector $\boldsymbol{\nu}$ satisfying $|\boldsymbol{\nu}| \leq 1$ [18]. In order to get existence, the denominators involving $|\nabla u|$ were replaced by $\sqrt{|\nabla u|^2 + \epsilon^2}$, and a limit extracted as $\epsilon \to 0$ [18]. As in the above theorem, terms like $\nabla u/|\nabla u|$ result in vectors $\boldsymbol{\nu}$ with modulus no greater than one, and satisfy a weak form of the equation.

4. Discrete Brakke Motions. The schemes proposed in the previous section a were motivated by integrating certain terms by parts, so satisfy (1) in a discrete distributional sense. While requiring such equations to hold in the sense of distributions is traditional in partial differential equations, this does not appear to be natural for geometric problems. To date, existence for flows by mean curvature have been obtained using the concept of viscosity solutions, or motion in the sense of Brakke [4]. As pointed out previously, the viscosity solution technique relies upon the maximum principle, so energy estimates are not particularly useful for this theory. However, the Brakke definition of motion by mean curvature is a weak statement very much in the spirit of a solution in the sense of distributions. In this section we show that (5) generates a discrete Brakke flow.

Since the definition of a Brakke flow is rather technical, we restrict our discussion to surfaces moving by mean curvature which are level sets of a function u. To introduce the ideas, we will assume that u is smooth and that it's gradient doesn't vanish. Adopting the notion of [19] we define

$$\boldsymbol{\nu} = \frac{\nabla u}{|\nabla u|}, \qquad \text{and} \qquad H = \nabla \cdot \boldsymbol{\nu}.$$

The level sets of u will then move by mean curvature in the sense of Brakke if for each $\phi \in C_0^1(\Omega)$, $\phi \geq 0$

$$\bar{D}_t \int_\Omega \phi |\nabla u| \leq - \int_\Omega (H^2 \phi + H \boldsymbol{\nu} \cdot \nabla \phi) |\nabla u|, \tag{10}$$

where $\bar{D}_t$ is the upper upper time derivative; $\bar{D}_t \psi(t) = \limsup_{s \to t} (\psi(t) - \psi(s))/(t-s)$. To see that this identity holds for smooth solutions of (1), note that $H = u_t/|\nabla u|$ and

$$\begin{aligned} \frac{d}{dt} \int_\Omega \phi |\nabla u| &= \int_\Omega \phi \boldsymbol{\nu} \cdot \nabla u_t \\ &= - \int_\Omega (H\phi + \boldsymbol{\nu} \cdot \nabla \phi) u_t \\ &= - \int_\Omega (H^2 \phi + H \boldsymbol{\nu} \cdot \nabla \phi) |\nabla u|. \end{aligned}$$

In the general setting considered by Brakke [4], the integrals of (10) become surface integrals[2], $\boldsymbol{\nu}$ is the approximate normal, $H\boldsymbol{\nu}$ is the mean curvature vector and H^2 is its magnitude.

[2] Recall that if $S = \{x \mid u(x) = c\}$ is a level set of u, then $\int_S f \, dA = \lim_{\epsilon \to 0} (1/2\epsilon) \int_{|u-c|<\epsilon} f |\nabla u| \, dx$.

To show that a discrete version of (10) holds for the first order scheme (5), we begin with a technical lemma.

LEMMA 4.1. *Let $\mathcal{T}_h$ be a triangulation of Ω, a_h be a non-negative piecewise constant function on $\mathcal{T}_h$, and define a the norm $\|.\|$ on $L^2(\Omega)$ by*

$$\|u\|^2 = \int_\Omega u^2/a_h.$$

For $\phi \geq 0$, $\phi \in C_0^2(\Omega)$ fixed, and $u_h \in V_h$, let $v = \phi u_h$ and $v_h = I_h(v) \in V_h$ be the nodal interpolant of v. Then there exists $C > 0$ such that

$$\|v - v_h\| \leq Ch^2(\|u_h\| + \|\sqrt{\phi}\nabla u_h\|),$$

and

$$\|\nabla(v - v_h)\| \leq Ch(\|u_h\| + \|\sqrt{\phi}\nabla u_h\|),$$

where $C = C(\phi)$ is independent of a_h, and the only mesh dependence is through the maximum ratio of diameter to largest inscribed sphere for any simplex.

Proof. Note that the hypotheses on ϕ guarantee that $\phi^{1/2} \in C_0^1(\Omega)$ [15]. Standard approximation theory shows that there is a constant C such that for any simplex $T \in \mathcal{T}_h$

$$\int_T (v - v_h)^2 \leq Ch^2 \int_T |D^2 v|^2 \qquad \text{and} \qquad \int_T |\nabla(v - v_h)|^2 \leq Ch \int_T |D^2 v|^2.$$

Since $v = \phi u_h$ and $u_h \in \mathcal{T}_h$, it follows that

$$|D^2 v| = |u_h D^2\phi + 2\nabla\phi \otimes \nabla u_h| = |u_h D^2\phi + \sqrt{\phi} 4\nabla\phi^{1/2} \otimes \nabla u_h| \leq C(|u_h| + |\sqrt{\phi}\nabla u_h|),$$

where $C = \max(\|D^2\phi\|_{L^\infty(\Omega)}, 4\|\nabla\phi^{1/2}\|_{L^\infty(\Omega)})$. The lemma now follows by dividing both sides of the estimate for a simplex by a_T, the value of a_h on T, and summing. □

THEOREM 4.2. *Let $u^{n+1} \in V_h$ be the solution of (5), and define H^{n+1} and $\boldsymbol{\nu}^{n+1}$ by*

$$H^{n+1} = \frac{2}{\tau} \frac{u^{n+1} - u^n}{|\nabla u^{n+1}| + |\nabla u^n|}. \qquad \text{and} \qquad \boldsymbol{\nu}^{n+1} = \frac{2\,\nabla u^{n+1}}{|\nabla u^{n+1}| + |\nabla u^n|}.$$

Fix $\phi \in C_0^2(\Omega)$, and suppose $\{\mathcal{T}_h\}$ is a regular family of meshes, then

$$\frac{1}{\tau}\int_\Omega (|\nabla u^{n+1}| - |\nabla u^n|)\phi \leq -\int_\Omega \left((H^{n+1})^2\phi + H^{n+1}\boldsymbol{\nu}^{n+1} \cdot \nabla\phi\right) \frac{1}{2}(|\nabla u^{n+1}| + |\nabla u^n|) + E(h, \tau; \phi),$$

where $E(h, \tau; \phi) \leq C(\phi)\tau^{1/2}$ provided h/τ remains bounded.

Proof. Recall that our existence results show that H^{n+1} and $\boldsymbol{\nu}^{n+1}$ are well defined even then the denominators vanish, and satisfy

$$\int_\Omega H^{n+1} v_h + \boldsymbol{\nu}^{n+1} \cdot \nabla v_h = 0 \qquad \forall\, v_h \in V_h.$$

Fix $\phi \in C_0^2(\Omega)$ and let $v = \phi(u^{n+1} - u^n)$ and $v_h = I_h(v)$ be the nodal interpolant of v on $\mathcal{T}_h$. Calculations similar to those in Section 2 show that

$$\begin{aligned}\frac{1}{\tau}\int_\Omega H^{n+1} v + \boldsymbol{\nu}^{n+1} \cdot \nabla v \;&=\; \int_\Omega \left((H^{n+1})^2\phi + H^{n+1}\boldsymbol{\nu}^{n+1} \cdot \nabla\phi\right)(1/2)(|\nabla u^{n+1}| + |\nabla u^n|) \\ &\quad + \frac{1}{\tau}\int_\Omega \left(|\nabla u^{n+1}| - |\nabla u^n| + \frac{|\nabla(u^{n+1} - u^n)|^2}{|\nabla u^{n+1}| + |\nabla u^n|}\right)\phi.\end{aligned}$$

Noting that we may replace v by $v - v_h$ on the left hand side we obtain

$$\frac{1}{\tau}\int_\Omega (|\nabla u^{n+1}| - |\nabla u^n|)\phi = -\int_\Omega \left((H^{n+1})^2\phi + H^{n+1}\boldsymbol{\nu}^{n+1}\cdot\nabla\phi\right)\frac{1}{2}(|\nabla u^{n+1}| + |\nabla u^n|) + E(h,\tau),$$

where

$$E(h,\tau) = \frac{1}{\tau}\int_\Omega \frac{2}{\tau}\frac{(u^{n+1}-u^n)(v-v_h)}{|\nabla u^{n+1}| + |\nabla u^n|} + 2\frac{\nabla u^{n+1}\cdot\nabla(v-v_h)}{|\nabla u^{n+1}| + |\nabla u^n|} - \frac{|\nabla(u^{n+1}-u^n)|^2}{|\nabla u^{n+1}| + |\nabla u^n|}\phi.$$

Define the weighted $L^2(\Omega)$ norm, $\|.\|$ by

$$\|u\|^2 = \int_\Omega \frac{2\,u^2}{|\nabla u^{n+1}| + |\nabla u^n|},$$

and recall that $\|u^{n+1} - u^n\|^2 \le \tau\|\nabla u_0\|_{L^1(\Omega)}$ and $\|\nabla u^{n+1}\|^2 \le \|\nabla u_0\|_{L^1(\Omega)}$. Applying the Cauchy–Schwarz inequality to the right hand side of the expression for the error gives

$$\begin{aligned} E(h,\tau) &\le \frac{1}{\tau}\left(\frac{1}{\tau}\|u^{n+1}-u^n\|\|v-v_h\| + \|\nabla u^{n+1}\|\|\nabla(v-v_h)\| - \frac{1}{2}\|\sqrt{\phi}\nabla(u^{n+1}-u^n)\|^2\right) \\ &\le \frac{1}{\tau}\|\nabla u_0\|^{1/2}_{L^1(\Omega)}\left(\frac{1}{\sqrt{\tau}}\|v-v_h\| + \|\nabla(v-v_h)\|\right) - \frac{1}{2\tau}\|\sqrt{\phi}\nabla(u^{n+1}-u^n)\|^2. \end{aligned}$$

An application of Lemma 4.1 shows

$$\begin{aligned} & E(h,\tau) \\ &\le C\|\nabla u_0\|^{1/2}_{L^1(\Omega)}\left(\frac{h^2}{\tau^{3/2}} + \frac{h}{\tau}\right)\left(\|u^{n+1}-u^n\| + \|\sqrt{\phi}\nabla(u^{n+1}-u^n)\|\right) - \frac{1}{2\tau}\|\sqrt{\phi}\nabla(u^{n+1}-u^n)\|^2 \\ &\le \tilde{C}\left(\sqrt{\tau} + \|\sqrt{\phi}\nabla(u^{n+1}-u^n)\|\right) - (1/2\tau)\|\sqrt{\phi}\nabla(u^{n+1}-u^n)\|^2 \\ &\le \tilde{C}\sqrt{\tau} + (\tilde{C}^2/2)\tau. \end{aligned}$$

□

Remarks: 1) It is tempting to select v_h as the projection

$$v_h \in V_h, \qquad \int_\Omega \frac{\nabla v_h\cdot\nabla w}{|\nabla u^{n+1}| + |\nabla u^n|} = \int_\Omega \frac{\nabla v\cdot\nabla w}{|\nabla u^{n+1}| + |\nabla u^n|} \qquad \forall\, w \in V_h,$$

instead of $I_h(v)$ in the proof above. While this eliminates the errors in the spatial term, we can't establish the second order error estimate for $v - v_h$ in the weighted $L^2(\Omega)$ norm (c.f. [27]). If the error is second order, then the above proof would extend to the second order scheme (3). Moreover, the error $E(h,\tau;\phi)$ for the first order scheme would satisfy $E(h,\tau;\phi) \le C(\phi)\tau$.
2) An analogous theorem for the lumped mass schemes is muddled by the fact that both H^{n+1}, as defined above, and the piecewise constant function having nodal values $H_i = (u_i^{n+1} - u_i^n)/|\nabla u_i|$ will appear.

5. Numerical Experiments. We limit our discussion to schemes (3) and (5) since we expect the corresponding lumped mass schemes (6) and (9) to behave similarly. Also, in order to avoid division by zero, terms of the form $|\nabla u|$ that were smaller than 10^{-7} were replaced by their epsilon approximants $|\nabla u|_\epsilon$ with $\epsilon = 10^{-9}$. This is motivated by our existence results above which obtained solutions by a similar technique.

5.1. Solution of the Implicit Equations. Each of the schemes are implicit, so require the solution of a nonlinear system of algebraic equations. We considered a natural relaxation scheme (given below) and Newton's method for the solution of these equations. Numerical experiments showed that the relaxation scheme applied to (5) was surprisingly robust; however, for (3) it failed to converge (or converged unacceptably slowly). Newton's scheme was extremely temperamental for both schemes. When it did converge, it did so rapidly; however, even with a good initial approximation obtained with the relaxation algorithm, convergence was not guaranteed. Accordingly, we only present results obtained using the relaxation algorithm applied to (5).

A natural iteration scheme for calculation of the solutions is to use the current guess to calculate the gradient terms in the denominator, and then let the updated guess be the solution of the corresponding linear equation. Specifically, set $u_{(0)} = u^n$, then for $k = 0, 1, 2, \ldots$, let $u_{(k+1)} \in V_h$ satisfy

$$\int_\Omega \frac{1}{\tau} \frac{(u_{(k+1)} - u^n)v}{|\nabla u_{(k)}| + |\nabla u^n|} + \frac{\nabla u_{(k+1)} \cdot \nabla v}{|\nabla u_{(k)}| + |\nabla u^n|} = 0, \qquad \forall\, v \in V_h, \tag{11}$$

for (5), with the obvious modification for (3). The difference between this relaxation scheme and Newton's algorithm is apparent if we let $\delta u = u_{(k+1)} - u_{(k)}$ and write (11) as

$$\int_\Omega \frac{1}{\tau} \frac{\delta u\, v}{|\nabla u_{(k)}| + |\nabla u^n|} + \frac{\nabla \delta u \cdot \nabla v}{|\nabla u_{(k)}| + |\nabla u^n|} = \int_\Omega F(u_{(k)}, v),$$

where

$$F(u, v) = \frac{1}{\tau} \frac{u - u^n}{|\nabla u| + |\nabla u^n|} v + \frac{\nabla u \cdot \nabla v}{|\nabla u| + |\nabla u^n|}.$$

Newton's scheme requires $\delta u \in V_h$ to satisfy

$$\int_\Omega \frac{1}{\tau} \frac{\delta u\, v}{|\nabla u_{(k)}| + |\nabla u^n|} + \frac{\nabla \delta u \cdot \nabla v}{|\nabla u_{(k)}| + |\nabla u^n|} - \left(\frac{F(u_{(k)}, v)}{|\nabla u_{(k)}| + |\nabla u^n|} \frac{\nabla u_{(k)} \cdot \nabla \delta u}{|\nabla u_{(k)}|} \right) = \int_\Omega F(u_{(k)}, v),$$

for all $v \in V_h$. A solution, u^{n+1}, of the equations will satisfy $\int_\Omega F(u^{n+1}, v) = 0$ for all $v \in V_h$. This suggests that $F(u^{n+1}, .)$ will be small, and if this is the case, the Jacobian matrix for Newton's method will be close to that used for the relaxation scheme.

When the mesh is strictly acute, the sequence $\{u_{(k)}\}$ generated by the relaxation scheme (11) is bounded in $L^\infty(\Omega)$, $\|u_{(k)}\|_{L^\infty(\Omega)} \le \|u^0\|_{L^\infty(\Omega)}$, provided τ is sufficiently large. It follows that $\{u_{(k)}\}$ will have a convergent sub–sequence, and numerical experiments indicated that the whole sequence usually converged. The $L^\infty(\Omega)$ bound follows from the fact that the denominators are non–negative, unlike the $W^{1,1}(\Omega)$ bounds which require the gradients in the denominator to match those in the numerator.

5.2. Boundary Conditions. Our discussion above assumed homogeneous boundary data. The extension for non–homogeneous Dirichlet data is relatively trivial. For example, if $\hat{u} \in W^{2,\infty}(Q)$, and we specify $u = \hat{u}$ on $\partial\Omega$, then the standard translation argument shows that the continuous problem satisfies the estimate

$$\frac{1}{2} \int_\Omega \frac{(u_t)^2}{|\nabla u|} + \frac{d}{dt} \|\nabla u\|_{L^1(\Omega)} \le \frac{1}{2} \|\hat{u}_t\|^2_{L^\infty(\Omega)} \| |\nabla u| \|_{L^1(\Omega)} + \|\nabla \hat{u}_t\|_{L^1(\Omega)}.$$

Gronwall's inequality then shows that $\|\nabla u(t)\|_{L^1(\Omega)}$ and $\iint (u_t)^2/|\nabla u|$ are bounded by the initial and boundary data. Discrete versions of these bounds are established in the obvious fashion.

The situation is quite different for non–homogeneous Neumann boundary data. Specifically, suppose that we consider the following weak problem for u:

$$\int_\Omega \frac{u_t}{|\nabla u|} v + \frac{\nabla u \cdot \nabla v}{|\nabla u|} = \int_{\partial\Omega} f v,$$

where $f = (1/|\nabla u|)\partial u/\partial n$ is boundary data. The a–priori bounds of Section 2 were obtained by selecting $v = u_t$, which may not have a well defined trace on the boundary. One can integrate by parts in time to get

$$\int_0^T \int_\Omega \frac{(u_t)^2}{|\nabla u|} + \|\nabla u(T)\|_{L^1(\Omega)} = \|\nabla u_0\|_{L^1(\Omega)} + \int_{\partial\Omega} (f(T)u(T) - f(0)u_0) + \int_0^T \int_{\partial\Omega} f_t u,$$

and the trace theorem can be used to estimate the right hand side. However, the bound $\int_{\partial\Omega} f(T)u(T) \le C\|f(T)\|_{L^\infty(\partial\Omega)}\|\nabla u(T)\|_{L^1(\Omega)}$ precludes the use of Gronwall's inequality unless $f(T)$ is very small. For example, the solutions are bounded when $f = 0$, as are the corresponding discrete solutions.

5.3. Examples.

5.3.1. Example 1: Regular Problem. We consider approximations of the radially symmetric solution of (1) given by

$$u(x,y) = e^{\left(-t-(x^2+y^2)/2\right)} - e^{-1/2}, \qquad 0 \le t \le 1, \tag{12}$$

on the unit square $[0,1]^2$. Note that the gradient vanishes at the origin, and we use rectangular meshes, so approximating this solution is not completely trivial. Meshes are constructed by dividing the square into similar rectangles and dividing them along the diagonal with negative slope. A 2×2 mesh is shown in Figure 2a. Figures 3 and 4 show the errors obtained by first holding the time step fixed and refining the mesh and then by fixing the mesh and varying the time step. The expected second order rates of convergence with respect to h and first order rates with respect to τ are clearly observed.

5.3.2. Example 2: Discontinuous Initial Data. If $\Phi : \Re \to \Re$ is a non–decreasing continuously differentiable function and u satisfies (1), then $\phi = \Phi(u)$ also satisfies (1). If we consider Φ close to the *sgn* graph[3] it is easy to verify that $\|\nabla\phi\|_{L^1(\Omega)} = \|\nabla\Phi(u)\|_{L^1(\Omega)}$ remains bounded by twice the perimeter of the zero set of u. In this situation we expect Ω to be partitioned into two regions where $\phi \simeq 1$ and $\phi \simeq -1$, with the interface between them moving by mean curvature. We consider numerical approximations of $\phi_\epsilon = \tanh(u/\epsilon)$, as $\epsilon \to 0$. For ϵ sufficiently small, the nodal values for the initial data will equal ± 1 to machine accuracy (except in the rare circumstance that computed value of u at a node is exactly zero). In this situation the best numerical approximation will have an interface with width h (or $2h$ if a nodal value is exactly zero). Figure 5 tabulates the errors for several values of ϵ, including

[3] $sgn(x) = 1$ if $x > 0$, -1 if $x < 0$ and $[-1,1]$ if $x = 0$.

$\epsilon = 0$ which corresponds to initial data taking on values of either ± 1. We consider the solution at $t = 15/32$, so that the zero set of u has moved from a radius of $r = 1$ at $t = 0$ to $r = 1/4$. For small values of ϵ, the relaxation scheme failed to converge (in 500 iterations) if the time steps were too large. While the average number of iterations per time step remained modest for small ϵ, certain steps required many more iterations than others. This is to be expected since the boundary values will jump from -1 to $+1$ when the zero set of u crosses them (the zero set being at radius $r(t) = \sqrt{1-2t}$).

5.3.3. Example 3: Neumann Boundary Data. Since the solution u, given in (12), is radially symmetric, the normal derivatives on the bottom and left hand sides of the square vanish. If we replace the (non-homogeneous) Dirichlet boundary data on these two sides with the homogeneous Neumann condition, the bounds established in Section 2 still apply. However, numerical problems were encountered when the Neumann condition was specified on two sides of the same element, as would be required at the origin with the mesh shown in Figure 2a. It was observed that the corner element would quickly attain a zero gradient and "lock up" in the sense that the discrete solution on this triangle wouldn't change. This behavior only polluted the solution in elements adjacent to offending corner, and it was observed that the solution still converged in $L^1(\Omega)$ as the mesh was refined. This problem could be avoided simply by changing the mesh so that the Neumann condition was required on at most one edge of an element as indicated in Figure 2b. Figure 6 shows contour plots of the discrete approximations of (12) obtained with a "good" and "bad" mesh. Note that there are theoretical subtleties associated with Neumann boundary conditions for degenerate second order equations [28]. In general, solutions will either satisfy the Neumann boundary data or satisfy the partial differential equation at a point on the boundary.

We repeat the calculations of Examples 1 and 2 with Neumann boundary conditions on the bottom and left hand sides of the square with "good" meshes. Figures 7–8 are the analogues of Figures 3–4 with the mixed boundary data. The first order rates of convergence with respect to τ are clearly observable for all of the norms. While the $W^{1,1}(\Omega)$ norm appears to converge at the expected linear rate with respect to h, the $L^\infty(\Omega)$ and $L^1(\Omega)$ norms do not appear to have attained an asymptotic rate. Figure 9 is the analogue of Figure 5 exhibiting behavior with discontinuous initial data. The relaxation scheme always converged with mixed boundary data; otherwise, the discrete solutions with Dirichlet and mixed boundary data exhibited similar trends. Figure 10 exhibits contour plots of the solutions obtained with $\epsilon = 0$ for each of the boundary conditions. As expected, the mixed boundary data results in considerably more smearing of the initially sharp interface.

5.3.4. Example 4: Fat Interface. Our final example exhibits the fattening of an initially sharp interface. The initial data is chosen to be $u^0(x,y) = dist((x,y), L)$, where $L = \{(x,0) \mid 0 \le x \le 1\} \cup \{(0,y) \mid 0 \le y \le 1\}$ is the set of points on the bottom and left hand sides of the unit square, i.e.

$$u^0(x,y) = \begin{cases} x & \text{if } x < y, \\ y & \text{otherwise.} \end{cases}$$

The solution was required to vanish on L for all times, and the homogeneous Neumann condition was specified on the remainder of the boundary. In this situation, the zero

set of u is initially L, and develops interior instantaneously. Our algorithm reproduces this phenomena as indicated in Figure 11 where the contours of the solution are plotted at $t = 1/4$.

6. Application to Other Problems. Many physical problems involving phase changes require the solution of a free surface problem. Typically a partial differential equation will be satisfied away from a free surface, and boundary conditions, which may involve curvature, are satisfied on the surface [6, 8, 20, 24, 23, 29, 38, 39]. A typical problem is the limit of the phase field equations [6] which may be written as

$$\frac{d}{dt}(cu + \ell\chi) - \Delta u = f, \qquad \text{in } \mathcal{D}'(\Omega), \tag{13}$$

$$v = \kappa + u, \qquad \text{on } \mathcal{S},$$

where $\chi = 1$ on the region interior of the region bounded by $\mathcal{S}$ and $\chi = 0$ on the region exterior to $\mathcal{S}$. v and κ are the normal velocity and mean curvature of the surface $\mathcal{S}$ respectively, and $c \geq 0$, $\ell > 0$, are physical constants. Requiring the equation for u to hold in the sense of distributions implies the usual jump condition $[\nabla u] \cdot \mathbf{n} = \ell v$, where $\mathbf{n}$ is the normal to $\mathcal{S}$. By introducing a function ϕ whose zero level set corresponds to $\mathcal{S}$, with $\phi > 0$ on the interior of $\mathcal{S}$, the free surface condition can be expressed as

$$\frac{1}{|\nabla\phi|}\frac{d\phi}{dt} = \nabla \cdot \left(\frac{\nabla\phi}{|\nabla\phi|}\right) + u \qquad \text{in } \Omega. \tag{14}$$

In this instance $\chi = H(\phi)$, the Heavyside function of ϕ. Formally, χ also satisfies (14), so multiplying (13) by u, and (14) by χ_t and adding the two gives

$$\frac{d}{dt}\int_\Omega \left(\frac{c}{2}u^2 + \ell|\nabla\chi|\right) + \int_\Omega \left(|\nabla u|^2 + \ell\frac{(\chi_t)^2}{|\nabla\chi|}\right) = 0,$$

showing that $\|u(t)\|_{L^2(\Omega)}$, $\|u\|_{L^2[0,T;H_0^1(\Omega)]}$ and $A(t)$ are all bounded, where $A(t)$ is the area of the free surface. Of course it is impossible to represent a Heavyside graph on a discrete mesh, so it is natural to approximate χ by ϕ, where the initial data for ϕ smears the sharp interface over one or two grid points. A numerical scheme analogous to (5) is: $(u^{n+1}, \phi^{n+1}) \in V_h \times V_h$

$$\int_\Omega \frac{1}{\tau}\left(c(u^{n+1} - u^n) + \ell(\phi^{n+1} - \phi^n)\right) v + \nabla u^{n+1} \cdot \nabla v = 0,$$

$$\int_\Omega \frac{2}{\tau}\frac{\phi^{n+1} - \phi^n}{|\nabla\phi^{m+1}| + |\nabla\phi^n|}\psi + 2\frac{\nabla\phi^{n+1} \cdot \nabla\psi}{|\nabla\phi^{m+1}| + |\nabla\phi^n|} = \int_\Omega u\psi,$$

for all $(v, \psi) \in V_h \times V_h$. This scheme will satisfy the natural energy estimate

$$\sum_{m=1}^{n}\int_\Omega \left(\frac{2}{\tau}\frac{\ell(\phi^m - \phi^{m-1})^2}{|\nabla\phi^m| + |\nabla\phi^{m-1}|} + \frac{\ell|\nabla(\phi^m - \phi^{m-1})|^2}{|\nabla\phi^m| + |\nabla\phi^{m-1}|} + |\nabla u^m|^2\right) +$$
$$+\frac{c}{2}\|u^n\|^2_{L^2(\Omega)} + \ell\|\nabla\phi^n\|_{L^1(\Omega)} \leq \frac{c}{2}\|u^0\|^2_{L^2(\Omega)} + \ell\|\nabla\phi^0\|_{L^1(\Omega)}.$$

Note that the solution is bounded even when $c = 0$ which arises when studying the Hele–Shaw instability [7, 40].

REFERENCES

[1] S. Angenent. Parabolic for curves on surfaces. I. curves with p–ingegrable curvature. *Ann. Math.*, 132:451–483, 1990.

[2] F. E. Baginski and N. Whitaker. Numerical solutions of boundary value problems for K surfaces in $\Re^3$. *Submitted*, 1993.

[3] G. Barles and P. Souganidis. Convergence of approximation schemes for fully nonlinear second order equations. *Preprint*, 1991.

[4] K. Brakke. *The Motion of a Surface by its Mean Curvature.* Mathematical Notes. Princeton University Press, 1978.

[5] L. Bronsard and R. Kohn. Motion by mean curvature as the singular limit of Ginzburgh–Landau model. *J. Diff. Eqns*, 90:211–237, 1991.

[6] G. Caginalp. An analysis of a phase field model of a free boundary. *Archive for Rational Mechanics and Analysis*, 92:205–245, 1986.

[7] G. Caginalp. Stefan and Hele–Shaw type models a assymptotic limits of phase field equations. *Physics Review A*, 39:887–896, 1989.

[8] G. Caginalp and E. A. Socolovsky. Efficient computation of a sharp interface by spreading via phase field methods. *Appl. Math. Let.*, 2/2:117–120, 1989.

[9] Y. G. Chen, Y. Giga, and S. Goto. Uniqueness and existence of viscosity solutions of generalized mean curvature flow equations. *J. Diff. Geom.*, 33:749–786, 1991.

[10] D. L. Chopp. Numerical computation of self–similar solutions for mean curvature flow. Technical Report LBL–34559, University of California, Aug. 1993.

[11] P. G. Ciarlet and P. A. Raviart. Maximum principle and uniform convergence for the finite element method. *Computer Methods in Applied Mechanics and Engineering*, 2:17–31, 1973.

[12] M. G. Crandall and P. L. Lions. Viscosity solutions of Hamilton–Jacobi equations. *Transaction AMS*, 277(1):1–42, 1983.

[13] K. Deckelnick and G. Dziuk. Convergence of a finite element method for non–parametric mean curvature flows. Technical Report 312, Bonn, Sept. 1993.

[14] E. DeGiorgi. Some conjectures on flow by mean curvature. In *Porceedings of Capri Workshop*, 1990.

[15] J. Dieudonné. Sur un théorème de glaeser. *Journal d'Analyse Mathematique*, 23:85–88, 1970.

[16] L. C. Evans. Convergence of an algorithm for mean curvature motion. *Preprint*, 1992.

[17] L. C. Evans, M. Soner, and P. E. Souganidis. Phase transistions and generalized motion by mean curvature. *Comm. Pure Appl. Math.*, 45:1097–1123, 1992.

[18] L. C. Evans and J. Spruck. Motion of level sets by mean curvature I. *J. Diff. Geom.*, 33:635–681, 1991.

[19] L. C. Evans and J. Spruck. Motion of level sets by mean curvature IV. *J. Geom. Analysis*, to appear, 1993.

[20] G. Fix. Phase field methods for free boundary problems. In B. Fasano and M. Primicerio, editors, *Free Boundary Problems*, pages 580–589. Pitman, London, 1983.

[21] P. M. Girao. Convergence of a crystalline algorithm for the motion of a simple closed convex curve by weighted mean curvature. *SIAM Journal on Numerical Analysis*, submitted, 1993.

[22] P. M. Girao and R. V. Kohn. Convergence of a crystalline algorithm for the heat equation in one dimension and for the mothion of a graph by weighted mean curvature. *Numerische Mathematik*, submitted, 1993.

[23] M. Gurtin and H. M. Soner. Some remarks on the Stefan problem with surface structure. Technical Report 90–92–NAMS–7, Carnegie Mellon University, Nov. 1990.

[24] M. E. Gurtin. Multiphase thermodynamics with interfacial structure, 1. Heat conduction and the capillary balance law. *Archive for Rational Mechanics and Analysis*, 104:195–221, 1988.

[25] T. Ilmanen. Convergence of the Allen–Cahn equation to Brakke's motion by mean curvature. *Preprint*, Nov. 1991.

[26] R. Jensen. The maximum principle for viscosity solutions of fully nonlinear second order partial differential equations. *Archive for Rational Mechanics and Analysis*, 101:1–27, 1988.

[27] C. Johnson and V. Thomée. Error estimates for a finite element approximation of a minimal surface. *Math. Comp.*, 29:343–349, 1975.

[28] M. Katsoulakis, G. Kossioris, and F. Retich. Generalized motion by mean curvature with Neumann conditions and the Allen–Cahn model for phase transitions. Technical Report 92-NA-036, Carnegie Mellon University, Oct. 1992.

Mesh	4×4	8×8	16×16	32×32	Norm
$L^\infty(\Omega)$ error	0.007852	0.002029	0.000526	0.000245	0.470337
$L^1(\Omega)$ error	0.001843	0.000394	0.000082	0.000081	0.337209
$W^{1,1}$ error	0.033204	0.013769	0.006506	0.003232	0.190741
Iterations/step	5.5	5.6	5.68	4.95	
τ/h	0.0283	0.0566	0.1131	0.2263	

FIG. 3. *Example 1: Solution at* $t = 1$, $\tau = 1/100$.

Time Step	1/10	1/20	1/40	1/80	Norm
$L^\infty(\Omega)$ error	0.002515	0.001276	0.000631	0.000309	0.470337
$L^1(\Omega)$ error	0.001035	0.000500	0.000233	0.000105	0.337209
$W^{1,1}$ error	0.006339	0.004157	0.003440	0.003254	0.190741
Iterations/step	14.6	11.75	9.275	5.525	
τ/h	2.2627	1.1314	0.5657	0.2828	

FIG. 4. *Example 1: Solution at* $t = 1$, 32×32 *mesh.*

[29] S. Luchaus. Solutions of the two phase Stefan problem with the Gibbs–Thomson law for the melting temperature. Technical Report 81, Bonn, Aug. 1989.

[30] R. H. MacNeal. An asymmetrical finite difference network. *Quarterly of Applied Math*, 11:295–310, 1953.

[31] R. H. Nochetto, M. Paolini, and C. Verdi. Optimal interface error estimates for the mean curvature flow. Technical Report 832, Pavia, 1992.

[32] S. Osher and J. Sethian. Fronts propagating with curvature dependent speed: Algorithms based on Hamilton Jacobi formulations. *Journal of Computational Physics*, 79:12–49, 1988.

[33] D. Otha, D. Jasnow, and K. Kawasaki. Universal scaling in the motion of a random interface. *Physics Review Letters*, 49:1223–1226, 1982.

[34] A. Roosen and J. Taylor. Simulation of crystal growth with facetted interfaces. *Mat. Res. Soc. Symp. Proc*, 237:25–36, 1992.

[35] J. A. Sethian. Numerical algorithms for propagating interfaces: Hamilton–Jacobi equations and conservation laws. *J. Diff. Geom.*, 31:131–161, 1990.

[36] J. A. Sethian and J. Strain. Crystal growth and dendrite solidification. *J. Comp. Phys.*, 98(2):231–253, 1992.

[37] H. M. Soner. Motion of a set by the curvature of its boundary. *Journal of Differential Equations*, 101/2:313–372, 1993.

[38] B. E. Stoth. Convergence of the Cahn–Hilliard equation to the Mullins–Sekerka problem in spherical symetry. Technical Report 298, Bonn, July 1993.

[39] J. E. Taylor, J. W. Cahn, and C. A. Handwerker. Geometric models of crystal growth. *Acta Met.*, 40:1443–1474, 1992.

[40] N. Whitaker. Some numerical methods for the Hele–Shaw equations. *Journal of Computational Physics*, Accepted, 1993.

ϵ	0.1	0.01	0.001	0.0001	0
$L^\infty(\Omega)$ error	0.017816	0.945311			
	0.009143	0.665379	1.999981		
	0.005011	0.489090	2.000000	2.000000	2.000000
$L^1(\Omega)$ error	0.003293	0.059355			
	0.001725	0.030190	0.178389		
	0.001012	0.019170	0.146915	0.187377	0.187348
$W^{1,1}$ error	0.040553	0.846847			
	0.033921	0.525918	2.475706		
	0.032283	0.370072	2.335205	2.158692	
$\|u\|_{L^1(\Omega)}$	0.757039	0.964624	0.996498	0.999867	1.000000

FIG. 5. *Example 2: Solution at $t = 15/32$, 32×32 mesh for 200 (top), 400 and 800 (bottom) time steps.*

Mesh	4×4	8×8	16×16	32×32	Norm
$L^\infty(\Omega)$ error	0.009343	0.003850	0.001783	0.001238	0.469908
$L^1(\Omega)$ error	0.003241	0.000322	0.000318	0.000359	0.337209
$W^{1,1}$ error	0.026656	0.010018	0.004643	0.002476	0.190741
Iterations/step	5.1	4.47	4.52	10.11	
τ/h	0.0283	0.0566	0.1131	0.2263	

FIG. 7. *Example 3: Solution of (12) at $t = 1$, $\tau = 1/100$ with mixed boundary data, Mesh 2.*

Time Step	1/10	1/20	1/40	1/80	1/160	Norm
$L^\infty(\Omega)$ error	0.011400	0.005915	0.002912	0.001509	0.000836	0.469908
$L^1(\Omega)$ error	0.004288	0.002093	0.000969	0.000455	0.000218	0.337209
$W^{1,1}$ error	0.011779	0.006311	0.003615	0.002618	0.002305	0.190741
Iterations/step	10.8	9.45	7.3	4.975	3.5	
τ/h	2.2627	1.1314	0.5657	0.2828	0.1414	

FIG. 8. *Example 3: Solution at $t = 1$, 32×32 mesh with mixed boundary data, Mesh 2.*

ϵ	0.1	0.01	0.001	0.0001	0
$L^\infty(\Omega)$ error	0.094850	1.895185	2.000000	2.000000	2.000000
	0.051566	1.200566	1.999887	2.000000	2.000000
	0.032863	0.917061	1.560559	1.644764	1.684151
$L^1(\Omega)$ error	0.031442	0.363090	0.543951	0.549184	0.589882
	0.017206	0.198779	0.329198	0.339603	0.361108
	0.010402	0.142109	0.219024	0.230409	0.237778
$W^{1,1}$ error	0.119800	2.301089	2.783140	2.604038	
	0.076891	1.397567	2.384789	2.222679	
	0.062293	1.208584	1.993385	1.910221	
$\|u\|_{L^1(\Omega)}$	0.757038	0.964617	0.996422	0.999770	1.000000

FIG. 9. *Example 3: Solution with mixed boundary data at $t = 15/32$, 32×32 mesh for 200 (top), 400 and 800 (bottom) time steps, Mesh 2.*

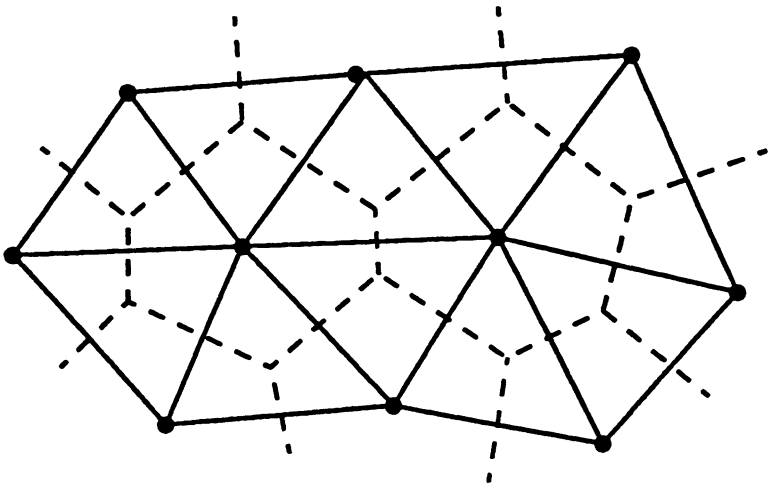

Figure 1. Complementary Volumes.

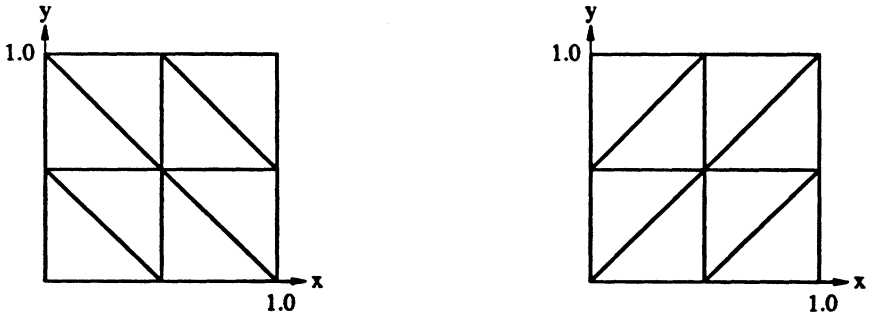

(a) Mesh 1 (b) Mesh 2

Figure 2. Meshes for Numerical Experiments

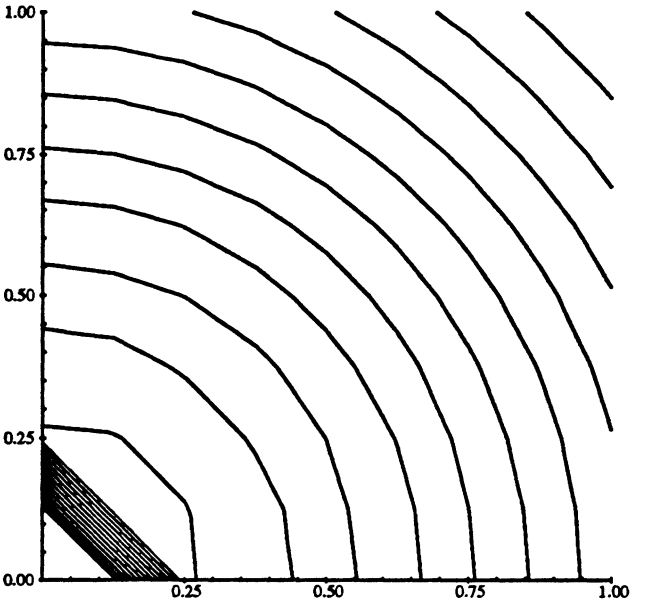

(a) Mesh 1, Contour Increment = 0.02

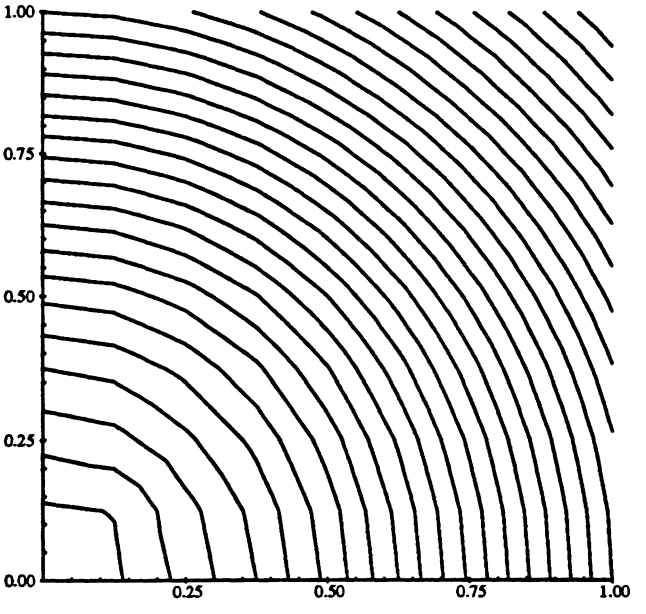

(b) Mesh 2, Contour Increment = 0.008

Figure 6. Mixed Boundary Conditions on 8x8 Meshes.

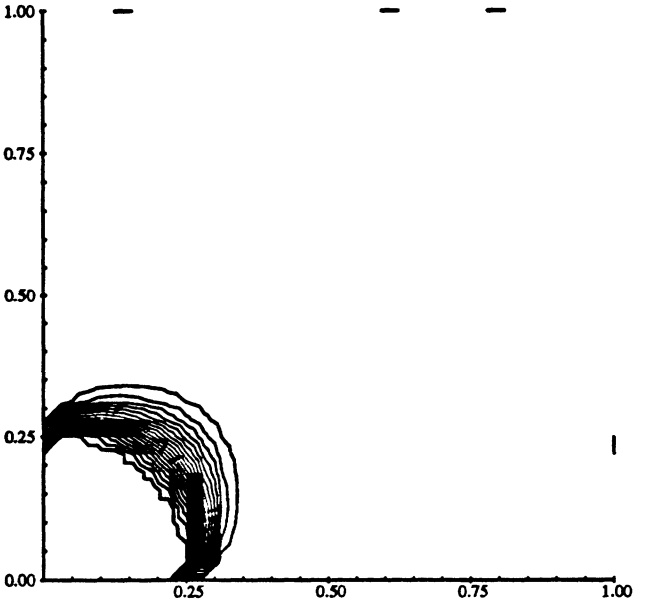

(a) Dirichlet Boundary Data, Contour Increment = 0.1

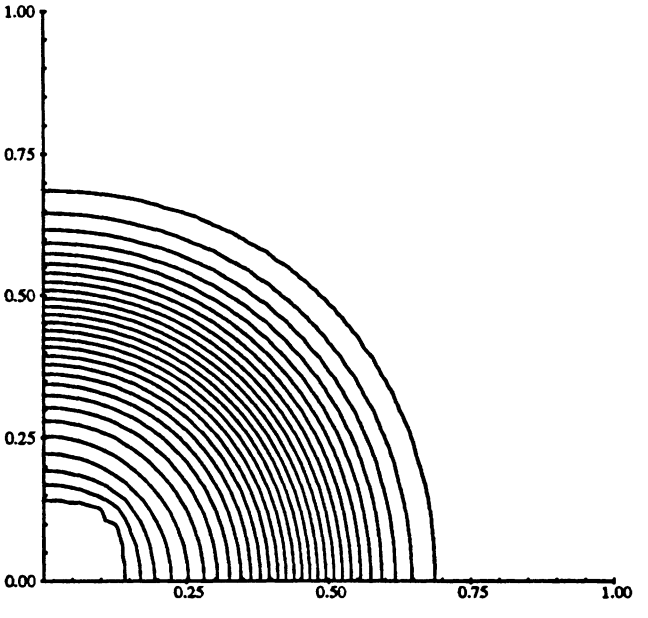

(b) Mixed Boundary Data, Contour Increment = 0.07

Figure 10. Example 3: 32x32 Mesh, 800 Time Steps, Mesh 2.

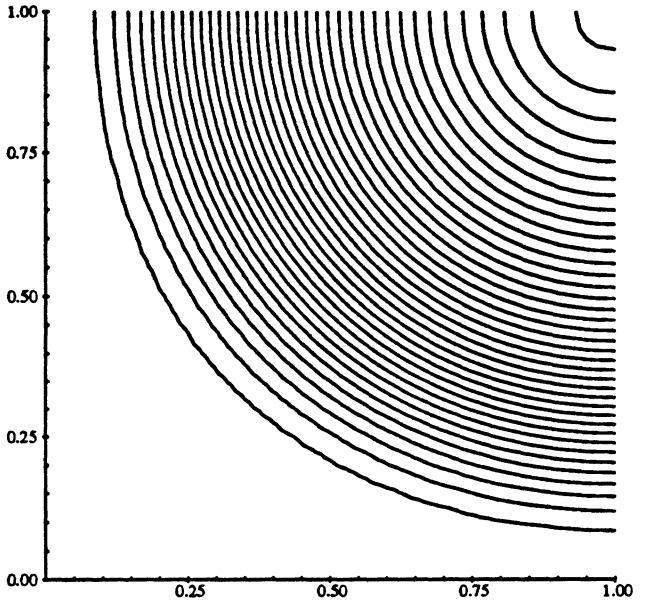

Figure 11. Example 4: 32x32 Mesh, 200 Time Steps
Contour Increment = 0.01, $0 < u < 0.375$.